Supporting information

Strontium Deficient Sr_xCoO_2-CoO_2 Nanotubes as a High Ampacity and High Conductivity Material

Kankona Singha Roy[1], Simon Hettler[2,3], Raul Arenal[2,3,4]* and Leela S. Panchakarla[1]

[1]*Department of Chemistry, Indian Institute of Technology Bombay, Powai, Mumbai, 400076, India.*

[2]*Instituto de Nanociencia y Materiales de Aragon (INMA), CSIC-Universidad de Zaragoza, Calle Pedro Cerbuna 12 - 50009 Zaragoza – Spain*

[3] *Laboratorio de Microscopias Avanzadas (LMA), Universidad de Zaragoza, Calle Mariano Esquillor, 50018 Zaragoza, Spain*

[4] *ARAID Foundation, 50018 Zaragoza, Spain*

*Corresponding email: *arenal@unizar.es

Content:

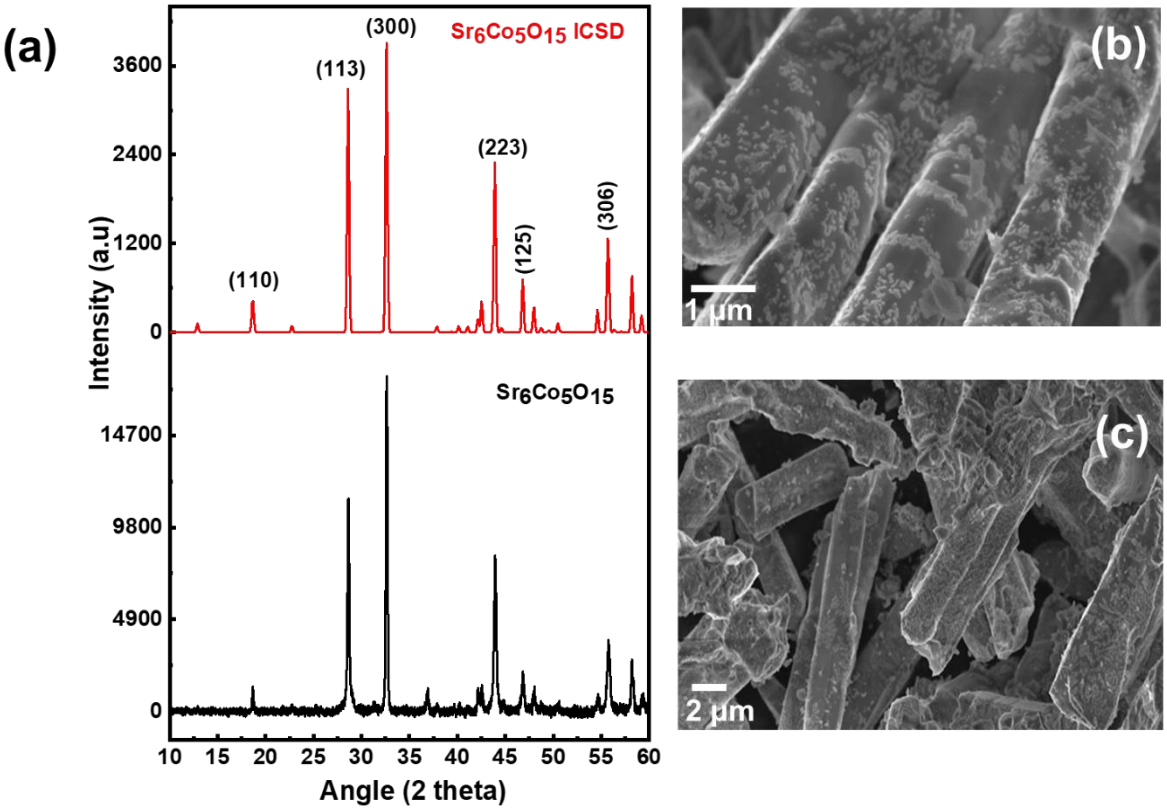

Figure S1: (a) Powder XRD patterns of as synthesised $Sr_6Co_5O_{15}$ and $Sr_6Co_5O_{15}$ from ICSD (coll code 81312). (b,c) SEM image of $Sr_6Co_5O_{15}$ bulk indicates a rod-like morphology.

X-ray diffraction (XRD) analysis of the bulk powder identifies the phase as $Sr_6Co_5O_{15}$ (SCO). The scanning electron microscopy (SEM) images of the as-prepared $Sr_6Co_5O_{15}$ show a rod-like morphology with a length varying from 5-20 µm and a width of 1-3 µm (**Figure S1(b,c)**).

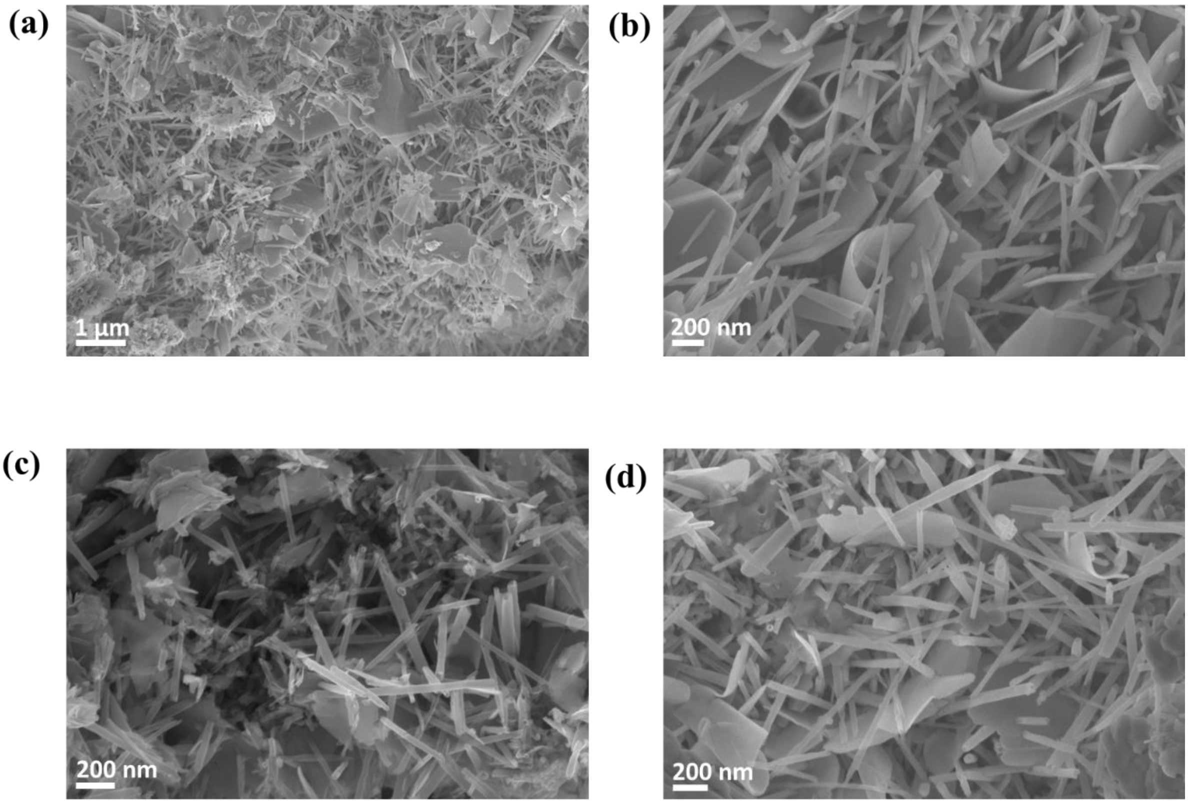

Figure S2: (a-d) SEM image of the nanotubes obtained after a reaction time of 12h.

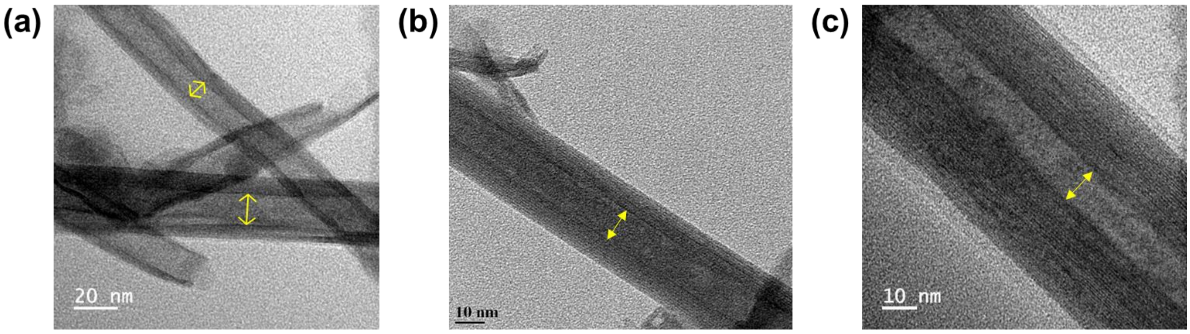

Figure S3: (a-c) TEM images of nanotubes where the double-sided yellow arrows indicate the hollow part of the nanotube.

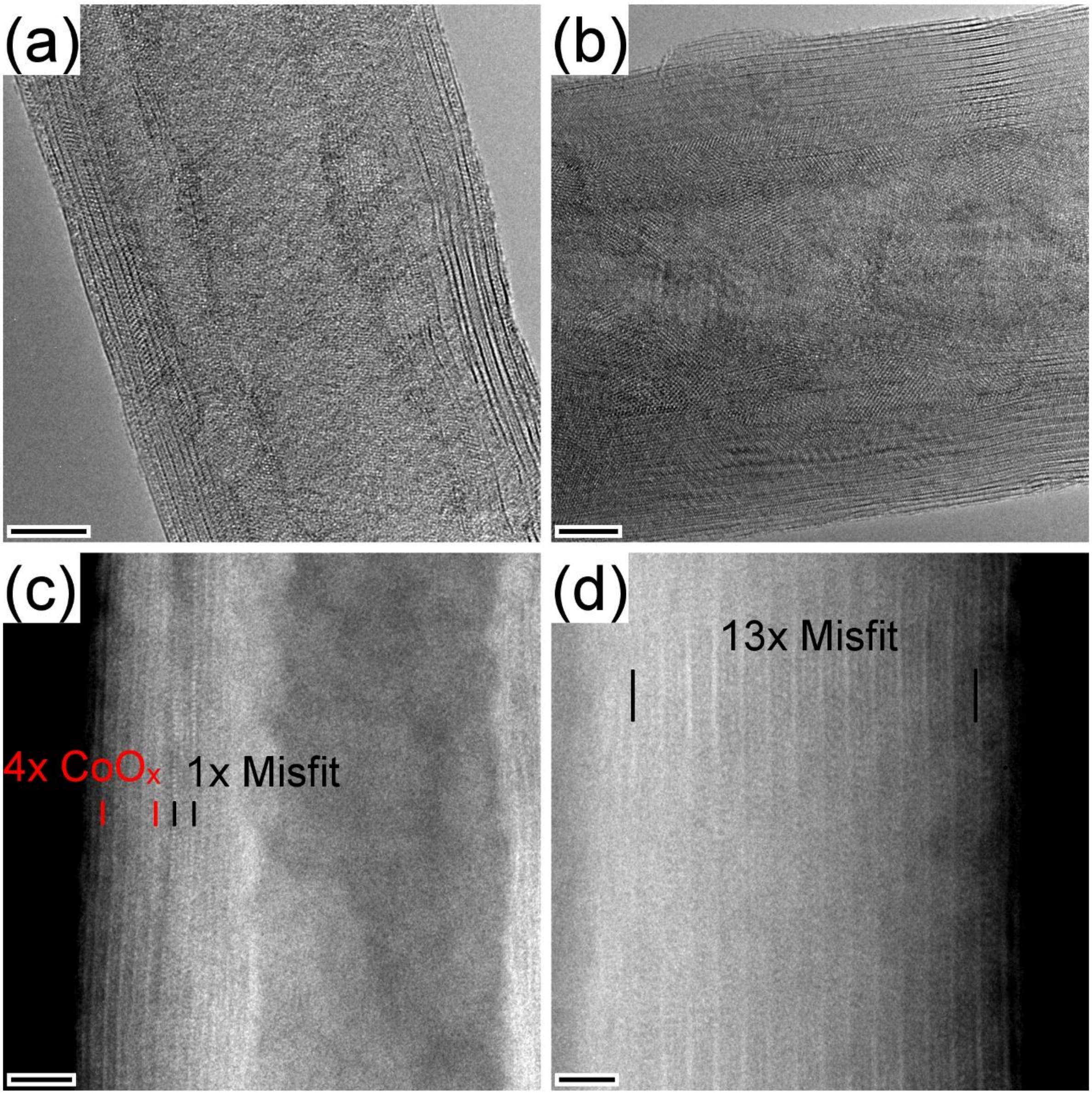

Figure S4: (a,b) Additional HRTEM images of SCO-NTs with varying wall thickness. Different d-spacings across the NT can be identified, which correspond to either the Misfit SCO or intercalated CoO_x lattice. While lattice fringes are mostly continuous in the NT imaged in (a), lattice fringes are bend and vary in contrast, which indicates local variations in the crystal structure between pure Misfit SCO and intercalated CoO_x planes. (c,d) Additional HR-STEM images of two SCO-NTs showing the varying amount of Misfit/intercalated CoO_x phase. CoO_x/Misfit structure dominates in (c)/(d), respectively. Scale bars are (a,b) 6 nm, (c) 3 nm and (d) 2 nm.

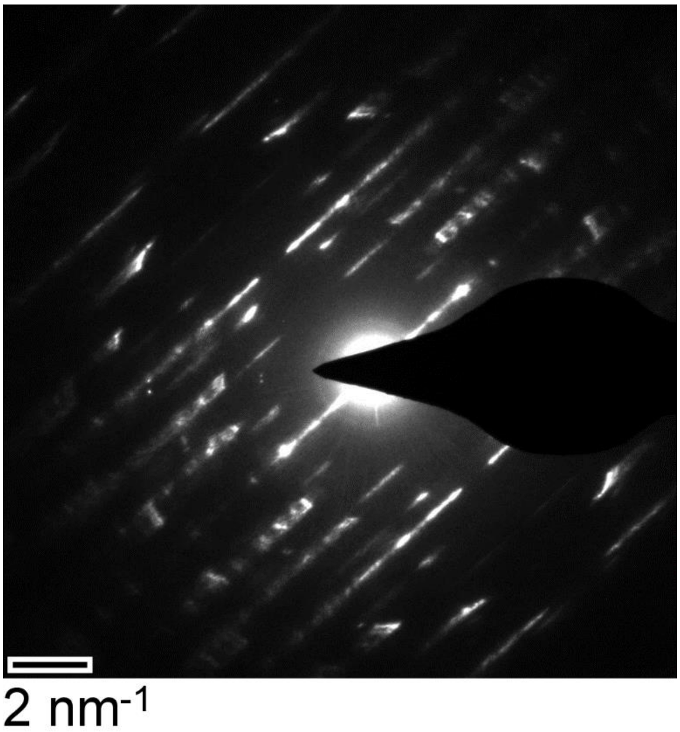

Figure S5: Diffraction pattern from Figure 2f without marks for reference.

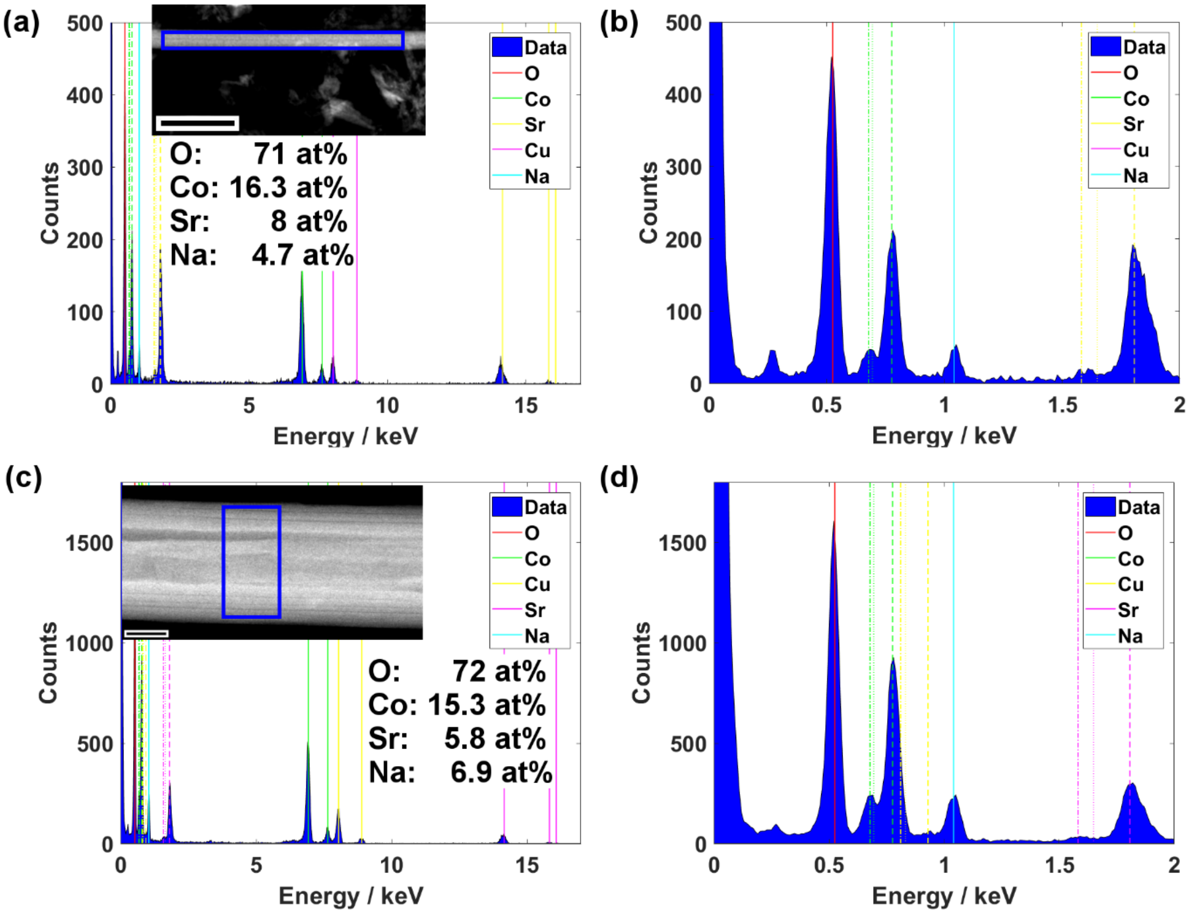

(e)	Oxygen	Cobalt	Strontium	Co + Sr	Natrium
Mean (min – max) composition / at%	73.2 (72 -74.8)	16.0 (14.1 – 17.5)	7.1 (5.3 – 9.5)	23 (22-24)	3.8 (3.2 – 4.7)

Figure S6: EDS-STEM analysis of two different SCO NTs. (a,b) Analysis of NT depicted in the inset image in (a) with the spectrum, acquired from the area marked blue, plotted for (a) a larger energy range up to 17 keV and (b) a smaller energy range better showing the low-energy peaks. (c,d) Analysis of NT depicted in inset image (c) with the spectrum again shown for (c) large and (d) smaller energy range. Peaks of Sr, Co, O and Na stem from the NT itself, while Cu originates from the support Cu grid. Solid lines correspond to the K-edges and dashed lines to L edges. Composition quantified using the K edges of the elements, not considering Cu, are plotted in (a and b). Scale bars are (a) 40 nm and (c) 20 nm. (e) Table with mean, minimum and maximum composition obtained from EDS analysis of 7 different NTs. While Co and Sr contents vary considerably (large differences between minimum and maximum values), the sum of both is rather constant.

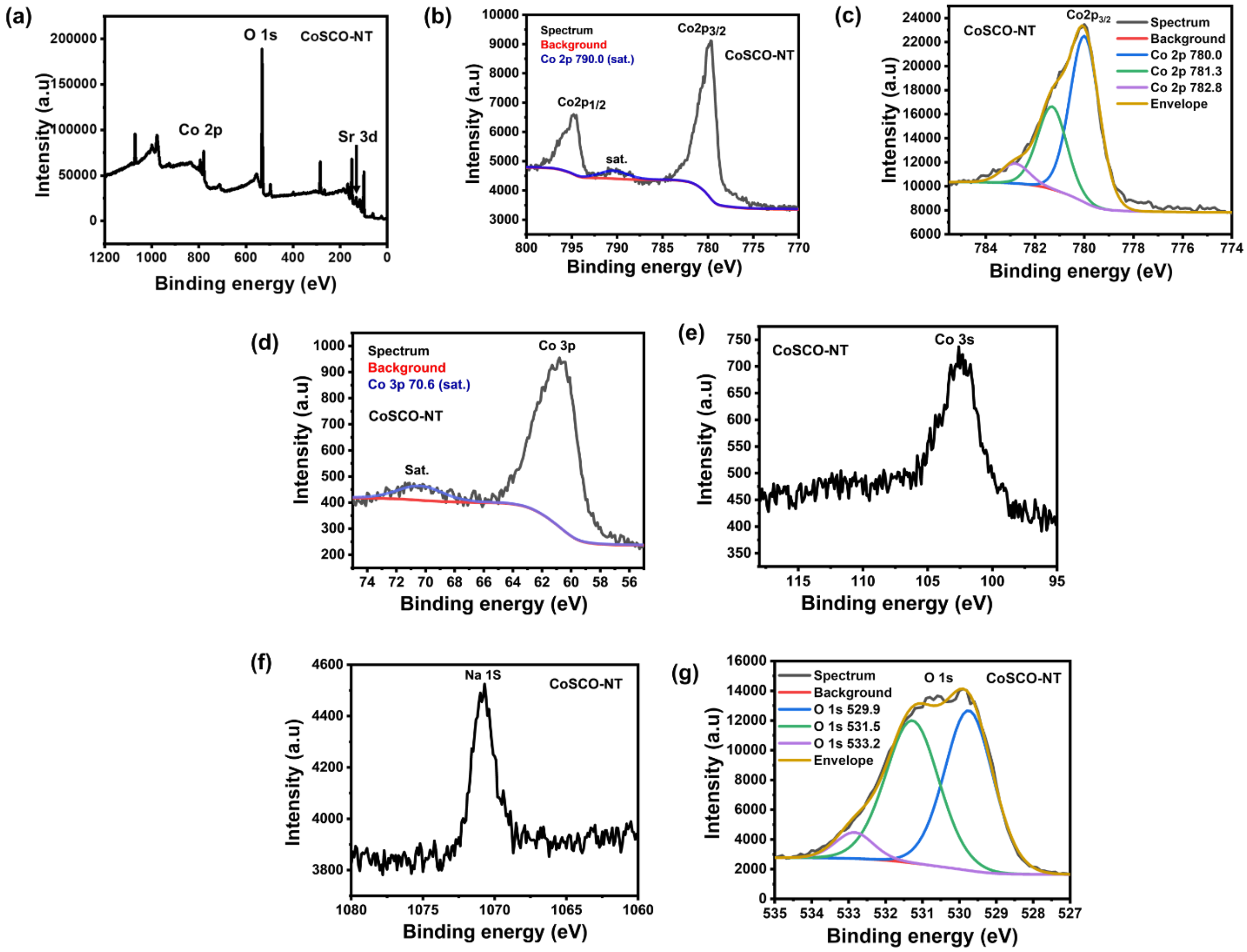

Figure S7: XPS analysis of SCO-NT. (a) XPS wide spectra indicating the presence of Sr 3d, Co 2p and O 1s. (b) XPS of Co 2p with the fitted satellite peak (overall fitting), (c) deconvoluted XPS spectra for Co $^2p_{3/2}$, (d) XPS spectra recorded for Co 3p with the fitted satellite peak (overall fitting), (e) XPS spectra of Co 3s, (f) XPS spectra of Na 1s, (g) deconvoluted XPS spectra for O 1s.

Table S1: Chemical state analysis of fitted XPS spectra for SCO-NT with percentage for (a) Co $2p_{3/2}$ and (b) O 1s.

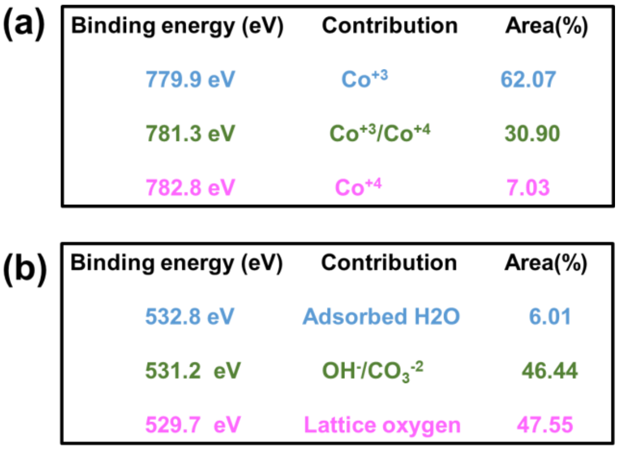

(a)

Binding energy (eV)	Contribution	Area(%)
779.9 eV	Co^{+3}	62.07
781.3 eV	Co^{+3}/Co^{+4}	30.90
782.8 eV	Co^{+4}	7.03

(b)

Binding energy (eV)	Contribution	Area(%)
532.8 eV	Adsorbed H2O	6.01
531.2 eV	OH^{-}/CO_3^{-2}	46.44
529.7 eV	Lattice oxygen	47.55

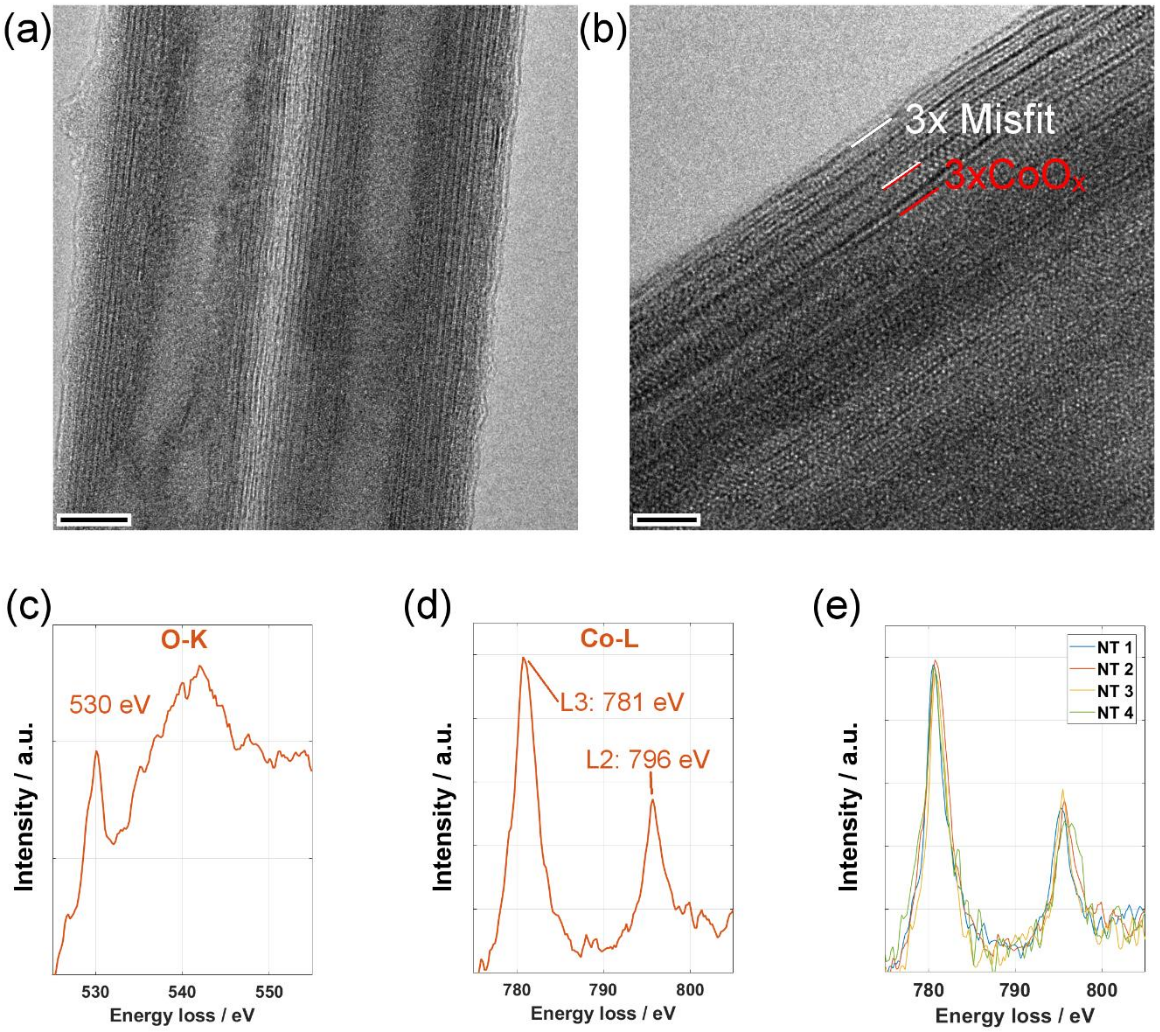

Figure S8: (a) TEM image of position for acquisition of EELS signal shown in (c,d), depicted ‘NT 2’ in €. (b) HRTEM image of NT depicted as ‘NT4’ in (e). (c) O-K Edge revealing sharp peak at 530 eV followed by a broad excitation between 535 -546 eV. (d) Co-L edge with L_3 peak at 781 eV and L2 at 796 eV. Please note that single-Gaussian fitting is not possible for both O-K peak at 530 eV and Co-L3 peak. (e) Comparison of Co-L Edge obtained from different NTs reveal homogeneous chemical environment for different NTs.

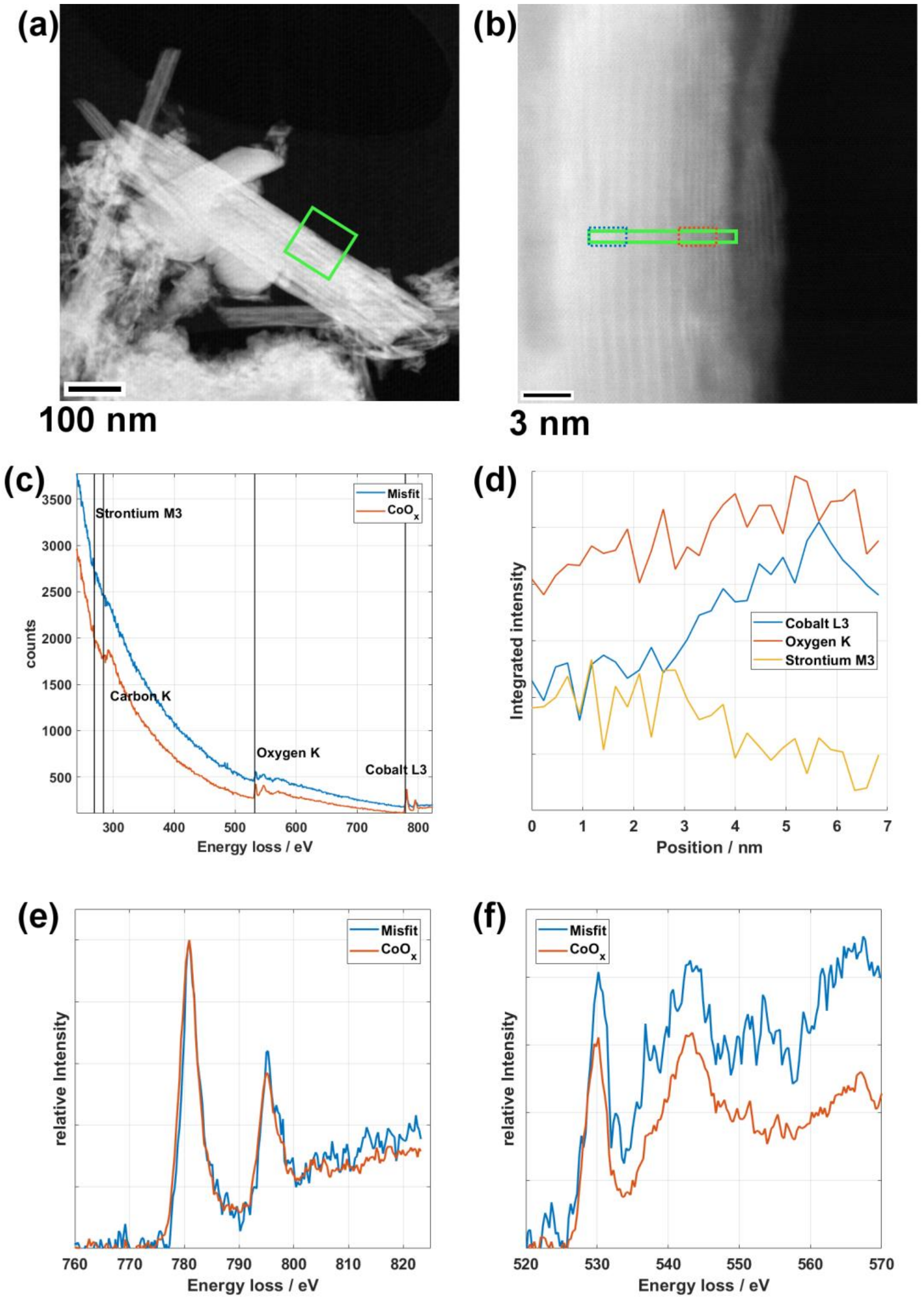

Figure S9: SR-EELS analysis of a SCO NT performed at 80 keV electron energy. (a) Overview dark-field image with region of image shown in (b) marked green. (b) HR-STEM image of the investigated area of the SCO NT with area used for SR-EELS analysis marked in green. Areas marked in blue and red correspond to the spectra designated as Misfit and CoO$_x$ in (c,e,f). (c) Overview spectra for Misfit and CoO$_x$ phases showing weak Sr-M$_3$, C-K (contamination), O-K and Co-L peaks. (d) Integrated intensities of Co L3 (blue), O K (red) and Sr-M$_3$ (yellow) showing an increase/decrease of Co/Sr intensity in the CoO$_x$ region. Integration was performed after power-law background subtraction using energy windows of 30 eV (Co, O) and 12 eV

(Sr, due to overlap with C-K edge). Comparison of background-subtracted spectra of Misfit and CoO_x regions for (e) Co-L and (f) O-K edges reveal small differences in the ELNES indicating minor changes in the valence in both region.

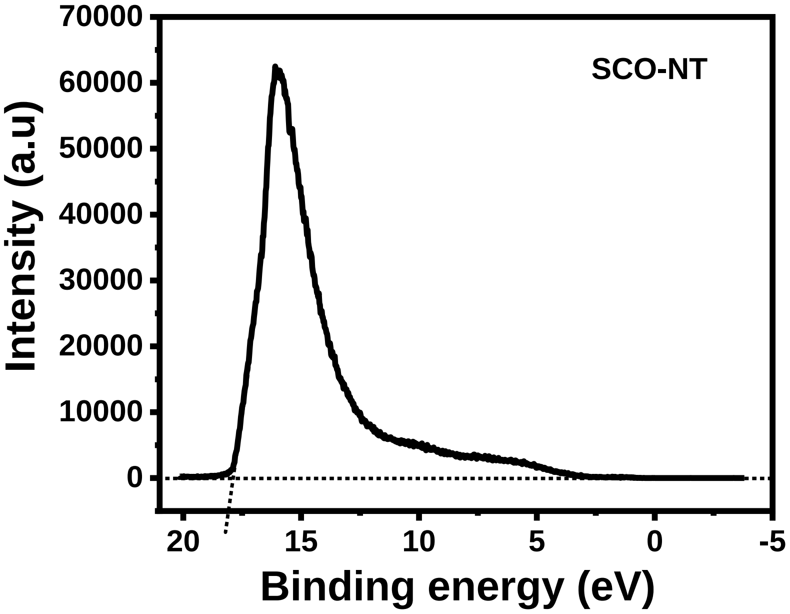

Figure S10: Ultraviolet photoelectron spectrum (UPS) of CoSCO-NTs.

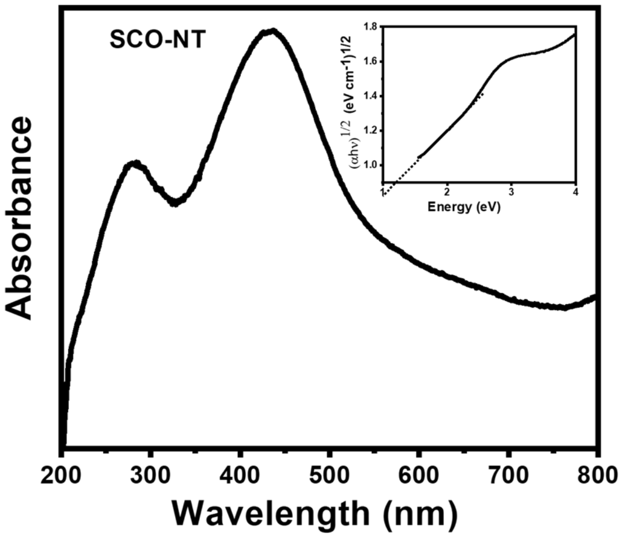

Figure S11: UV-Vis spectra recorded for SCO-NTs and the inset graph shows the Tauc plot.

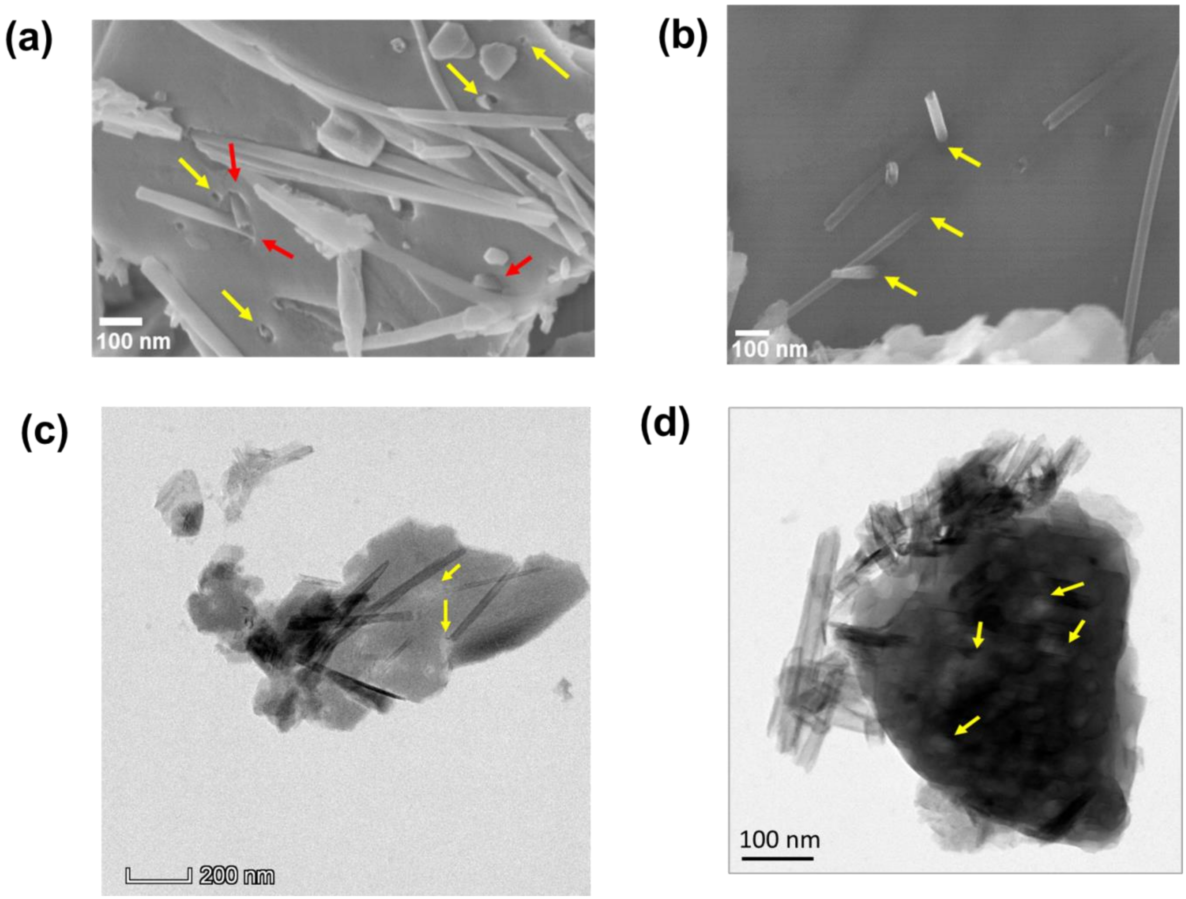

Figure S12: (a,b) SEM images during the growth of the nanotubes, (c,d) Low magnification TEM images during the growth period.

Figure S12(a,b) shows the SEM image of SCO-NTs for a reaction time of 6h. Yellow arrows shows the growth points from where the nanotubes are coming out of the bulk and red arrow marks indicates the grown NT from bulk. TEM images show low contrast regions from where the tubes are growing (**Figure S12(c,d)**).

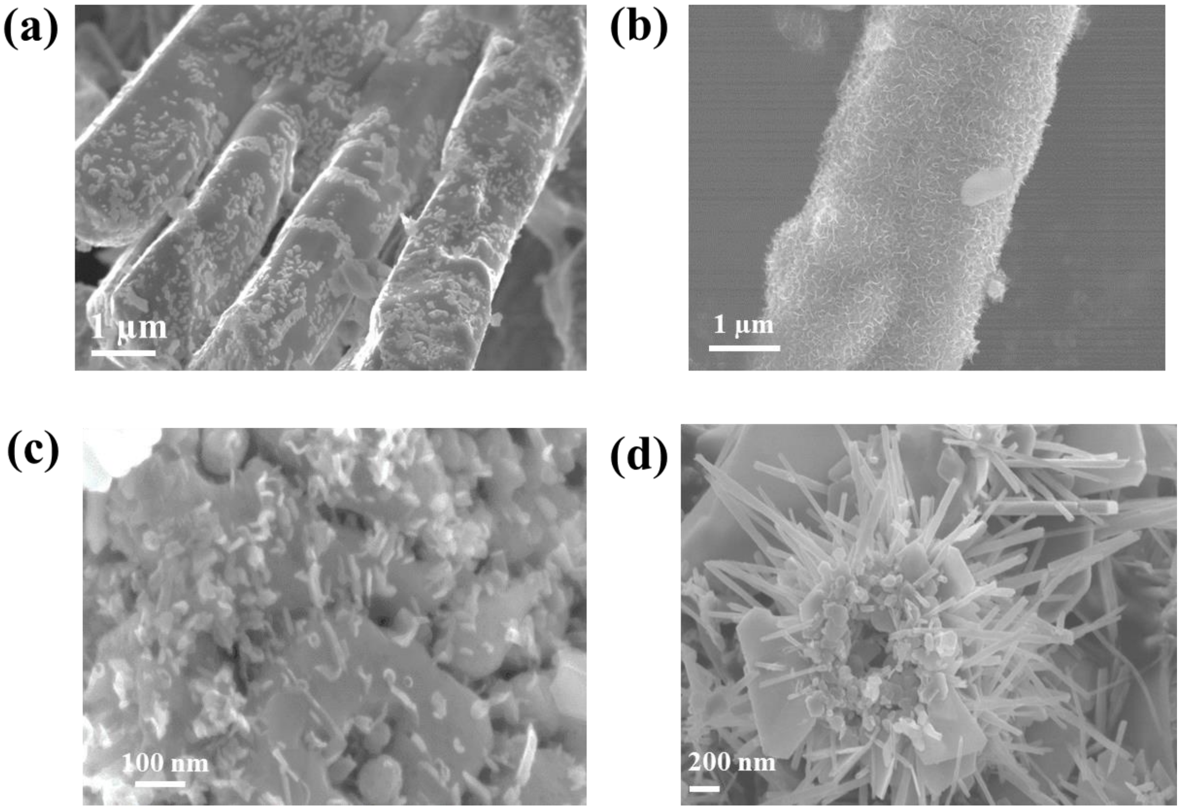

Figure S13: SEM images illustrating the growth of nanotubes obtained at (a) 0h (parent bulk), (b) 1h, (c) 3h and (d) 10h, respectively.

Figure S13 clearly helps to further understand the conversion of the pseudo-one-dimensional crystal structure in bulk (rod-like morphology) into 2D Sr-leached CoO rich bulk, which is inducing the nanotube growth. **Figure S13a** shows the rod-like morphology for bulk $Sr_6Co_5O_{15}$, from where the etching of SrO layer is taking place during the initial time of reaction (1h) as observed in Fig S13b. Upon the leaching of SrO layer, the face sharing octahedra chains in bulk $Sr_6Co_5O_{15}$ become unstable and convert themselves into 2D bulk-like morphology which is Sr-leached CoO_x (Fig 3e-f). As seen in **Figure S13c**, the nanotube growth (very small) has been spotted after 3h of reaction on the surface of Sr-leached CoO_x. After 6h, the nanotubes are clearly seen to be coming out of the 2d Sr-leached CoO_x (**Figure 3a-d**). This nanotube growth could be driven by more stable structural form of Sr_xCoO_2-CoO_2 (Sr deficient misfit) which is energetically more favorable. With longer duration (10h) the complete original bulk rod seems to have been converted into the nanotubular phase as seen from **Figure S13d**.

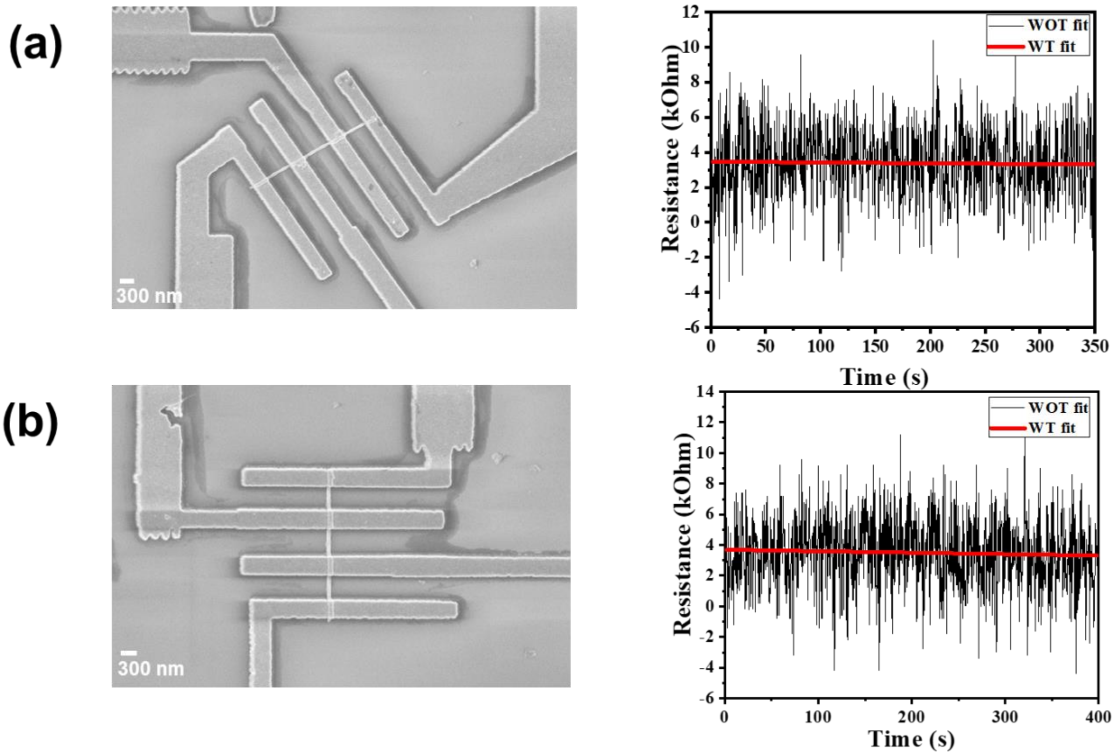

Figure S14: (a,b) SEM images of a four-probe device for a single SCO-NT and the corresponding resistivity (R) vs time (t) graph implies the stability of current over time.

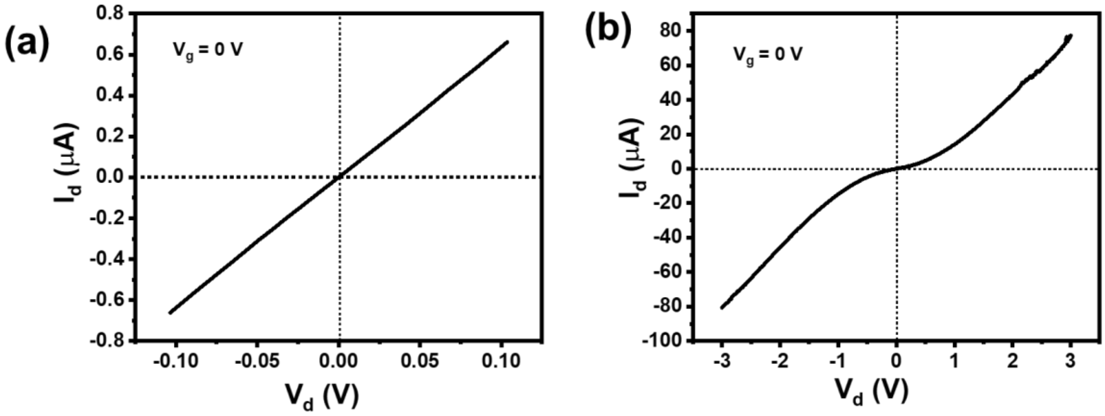

Figure S15: I_d-V_d graph of a typical two probe device (a) for a low voltage region (V_g = 0 V), and (b) for a voltage region of -3 V to 3 V.

(a)

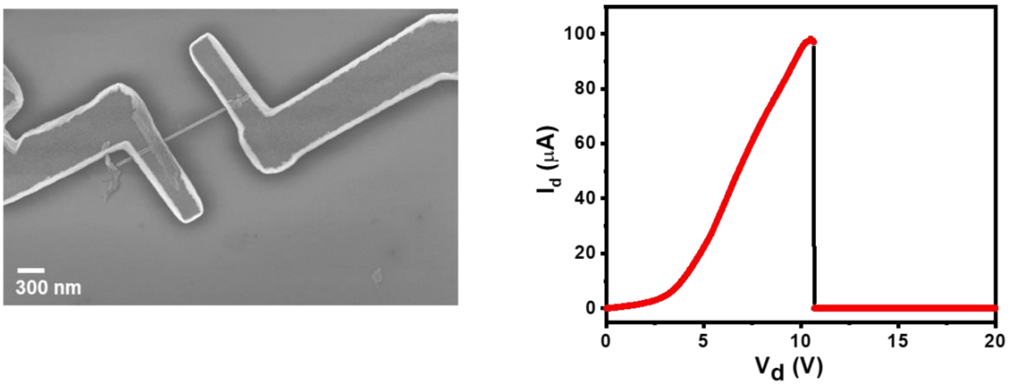
300 nm
I_d (μA)
0
20
40
60
80
100
0
5
10
15
20
V_d (V)

(b)

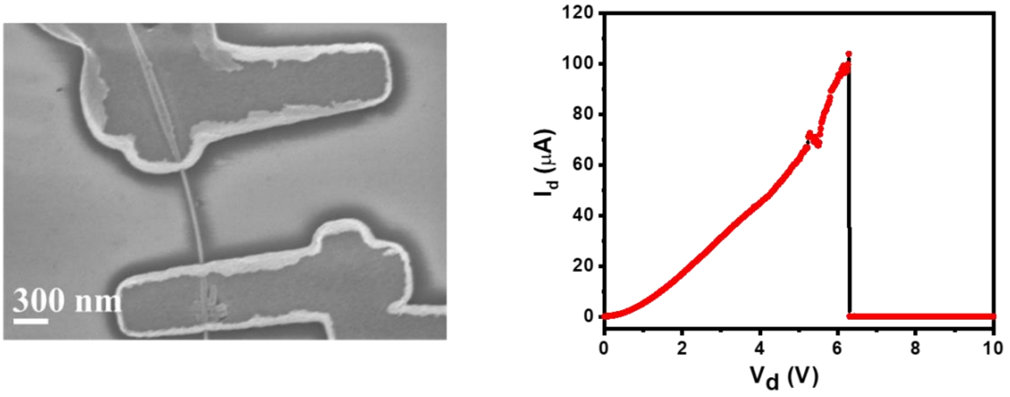
300 nm
I_d (μA)
0
20
40
60
80
100
120
0
2
4
6
8
10
V_d (V)

(c)

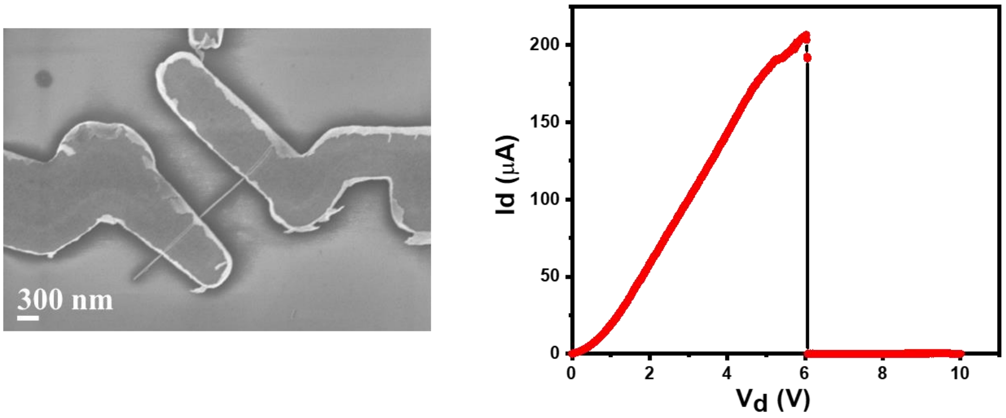
300 nm
Id (μA)
0
50
100
150
200
0
2
4
6
8
10
V_d (V)

(d)

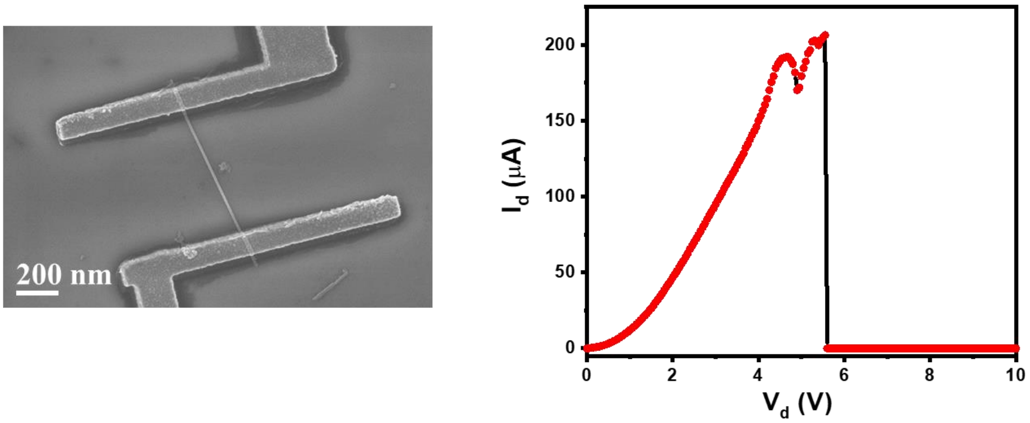
200 nm
I_d (μA)
0
50
100
150
200
0
2
4
6
8
10
V_d (V)

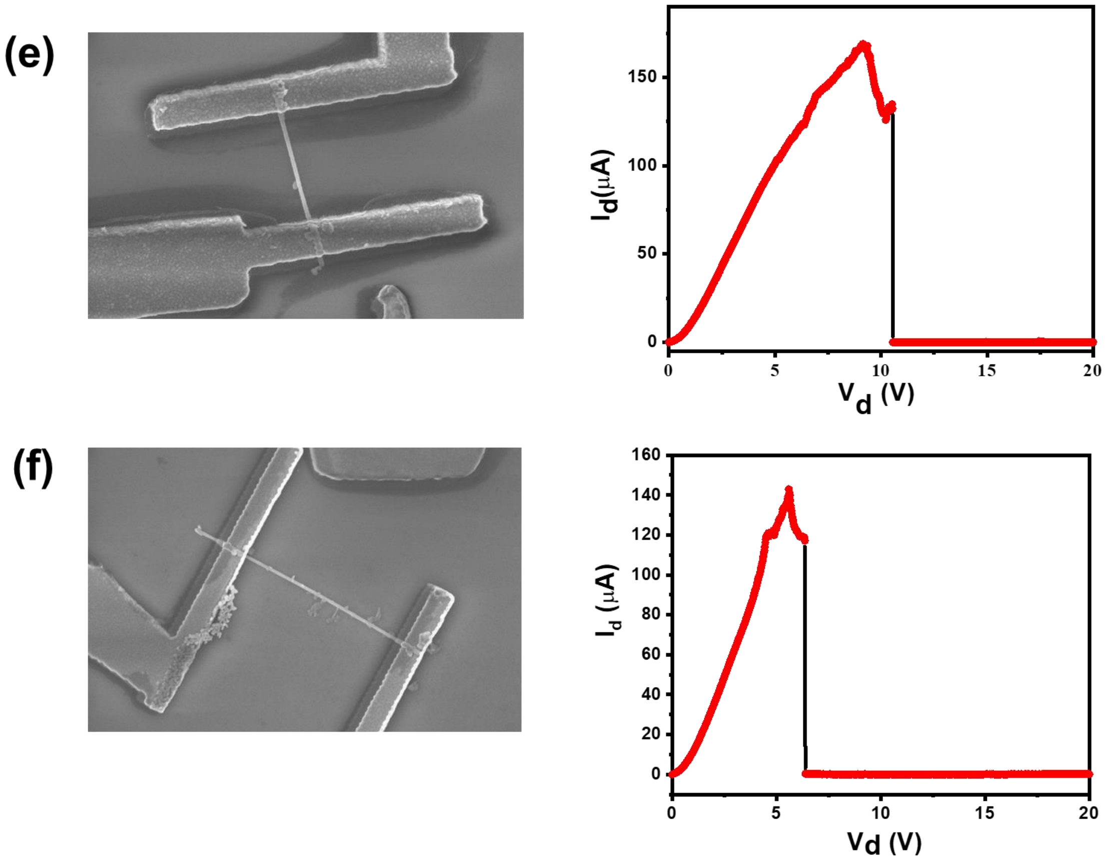

Figure S16: (a-f) SEM images of six different two probe devices and their corresponding I_d-V_d graphs till the breakdown ($V_g = 0$ V). The ampacity of device (a) - (f) is found to be:

(a) 0.14×10^8 A/cm^2 (breakdown voltage 10.2 V),

(b) 0.18×10^8 A/cm^2 (breakdown voltage 6.1 V),

(c) 0.21×10^8 A/cm^2 (breakdown voltage 6.05 V),

(d) 0.76×10^8 A/cm^2 (breakdown voltage 5.6 V),

(e) 0.27×10^8 A/cm^2 (breakdown voltage 10.5 V) and

(f) 0.127×10^8 A/cm^2 (breakdown voltage 6.44 V) respectively.

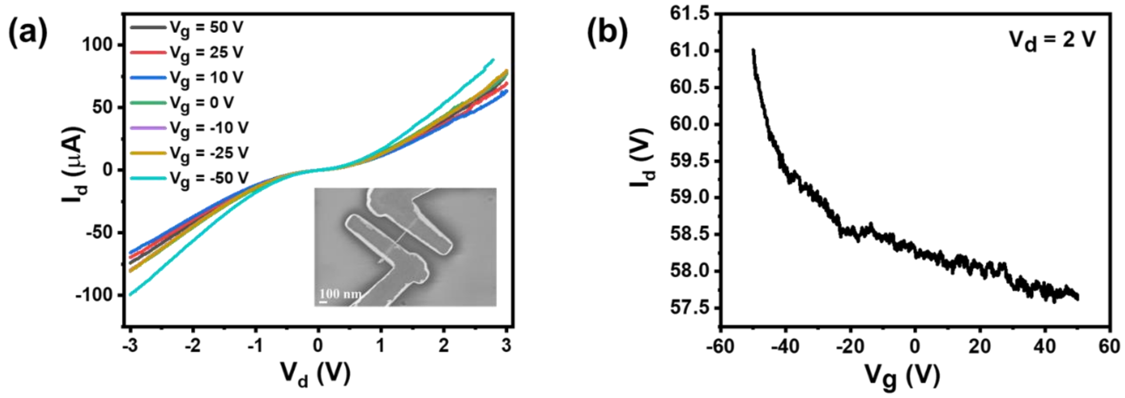

Figure S17: (a) Output characteristics of a typical two probe device (inset shows the SEM image of the device) and (b) transfer characteristics of the same device which gives a mobility value of 0.7 cm^2.V^{-1}·s^{-1}.

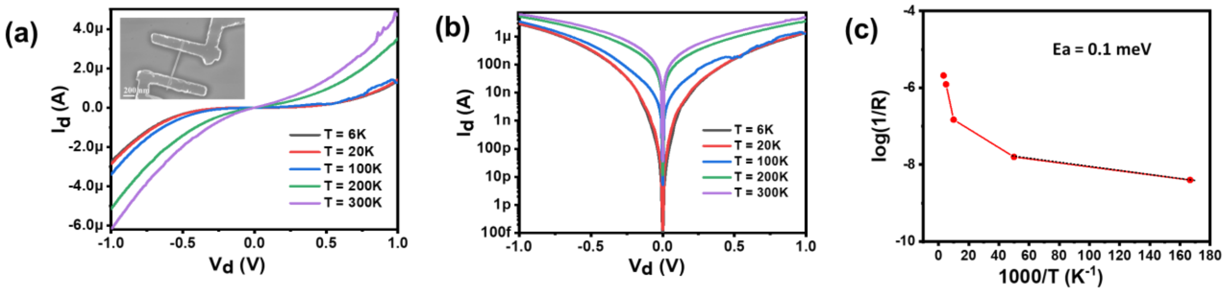

Figure S18: (a) Temperature-dependent I_d-V_d graph for SCO-NT ranging from 6 k to 300 K. (b) logI_d vs V_d of the device presented in the (a) indicating ohmic contact and small barrier heights for current flow despite large contact resistances. (c) Arrhenius plot giving the activation energy (E_g) 0.1 meV.

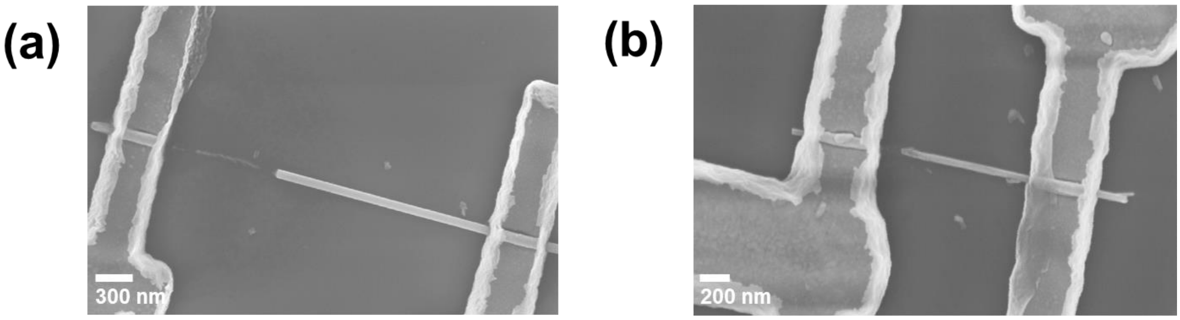

Figure S19: (a,b) SEM images of SCO-NT two-probe devices after the breakdown.

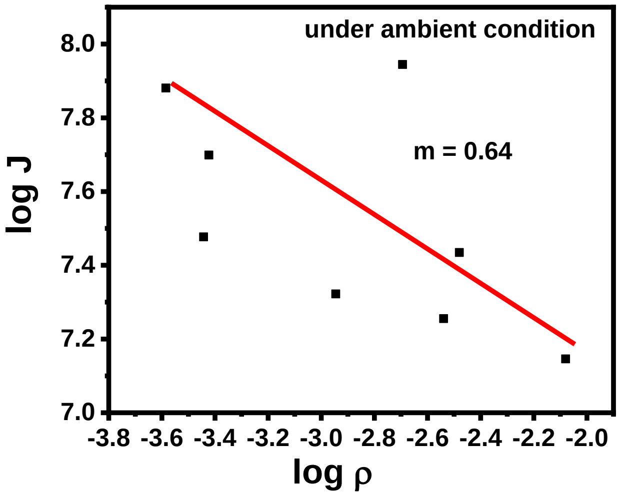

Figure S20: Plot of logJ vs logρ (according to power-law), which determines the breakdown mechanism.

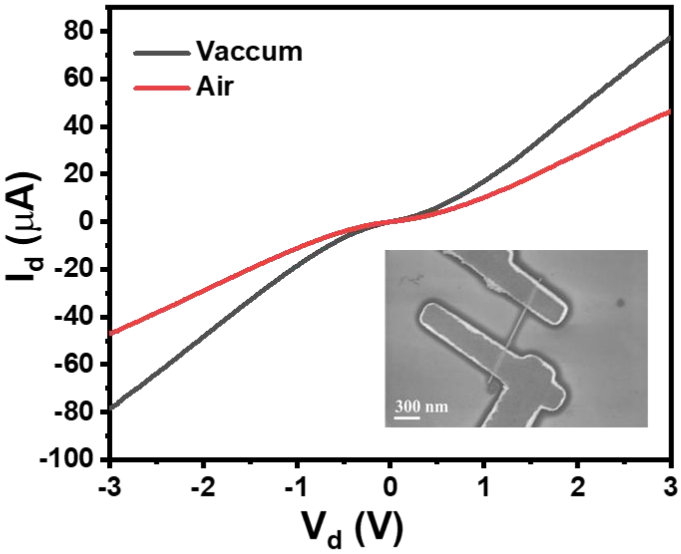

Figure S21: Comparison of drain current (I_d) at a zero-gate voltage (V_g) for a two probe device (inset) under vacuum and ambient atmosphere.

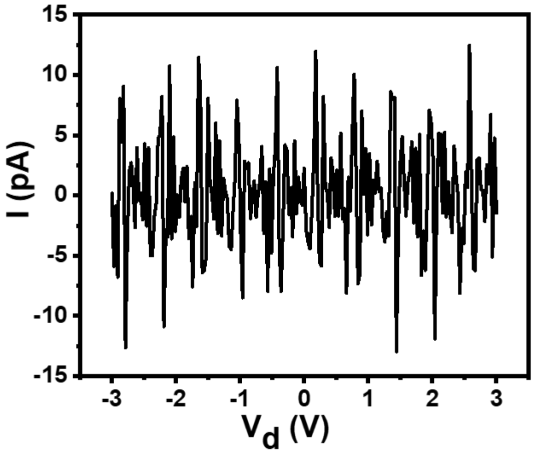

Figure S22: I_d vs V_d for a two-probe device with no nanotubes in between the electrodes, which suggests the current passes through the nanotube, not from the substrate.

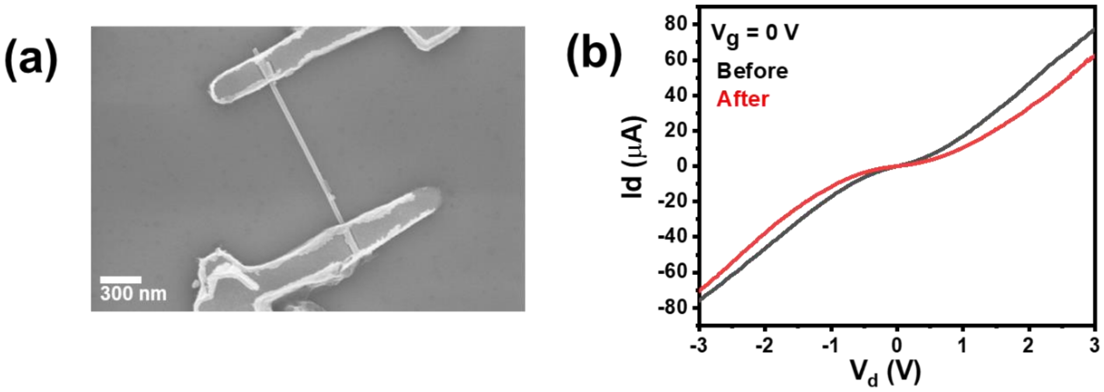

Figure S23: (a,b) Sustainability of the devices under ambient temperature and pressure for tested 10 months. (a) SEM image of a device after 10 months and (b) comparison of drain current (V_g = 0 V) before and after 10 months.